Impacts of random filling on spin squeezing via Rydberg dressing in optical clocks

Jacques Van Damme, Xin Zheng, Mark Saffman, Maxim G. Vavilov, and Shimon Kolkowitz

Phys. Rev. A **103**, 023106 — Published 11 February 2021

DOI: 10.1103/PhysRevA.103.023106

Impacts of Random Filling on Spin Squeezing via Rydberg Dressing in Optical Clocks

Jacques Van Damme, Xin Zheng, Mark Saffman, Maxim G. Vavilov, and Shimon Kolkowitz*
Department of Physics, University of Wisconsin - Madison, Madison, WI 53706
(Dated: January 22, 2021)

We analyze spin squeezing via Rydberg dressing in optical lattice clocks with random fractional filling. We compare the achievable clock stability in different lattice geometries, including unity-filled tweezer clock arrays and fractionally filled lattice clocks with varying dimensionality. We provide practical considerations and useful tools in the form of approximate analytical expressions and fitting functions to aid in the experimental implementation of Rydberg-dressed spin squeezing. We demonstrate that spin squeezing via Rydberg dressing in one-, two-, and three-dimensional optical lattices can provide significant improvements in stability in the presence of random fractional filling.

I. INTRODUCTION

Since their advent roughly seven decades ago, atomic clocks have developed at a rapid pace. State-of-the-art optical lattice clocks are now operating at or near the standard quantum projection noise (QPN) limit [1–4], particularly in differential clock comparisons where correlated noise spectroscopy can be employed to remove local oscillator noise [3, 5–8]. High precision clock comparisons can be used for exciting applications such as tests of relativity [9], searches for dark matter [10], tracking of space-craft [11], and relativistic geodesy [12]. Further improvements in clock stability will enhance their use for these applications, and will open the door to new applications in searches for beyond Standard Model physics and gravitational wave detection [13, 14].

The QPN limit arises from the independent projection onto the clock state basis of each of the atoms used to reference the local oscillator. Introducing entanglement between the atoms in the form of spin squeezing can reduce the uncertainty associated with these measurements [15–17]. A high degree of spin-state squeezing in large atom ensembles and optical lattice clocks has been demonstrated using coupling of the atoms to an optical cavity [18, 19]. Recently, an attractive alternative approach was proposed in which the squeezing is generated through dressed Rydberg interactions that can be turned on and off with one additional laser [20], and there have been subsequent demonstrations of the one-axis twisting Hamiltonian using dressed Rydberg interactions in alkali atoms [21], as well as the generation of entangled Bell states in pairs of strontium atoms using the same transitions [22]. However, spin-squeezing of an optical clock transition via Rydberg-dressing has yet to be experimentally demonstrated, and there are a number of important practical considerations that have not previously been investigated.

There are now three different geometric configurations of neutral atom optical clocks. In most current optical lattice clocks a roughly 10^3-10^4 site one-dimensional lattice is loaded stochastically from a magneto-optical trap (MOT). The resulting random variations in the number of atoms occupying each site can result in dephasing due to on-site atom-atom interactions at high atom densities [23] or a lattice filling fraction $P_{\text{filling}} < 1$ in the low-density regime. A recently demonstrated alternative approach makes use of evaporative cooling to load Fermi-degenerate atoms into a three-dimensional lattice with a filling fraction approaching unity [3, 4, 24]. Finally, there have been recent demonstrations of tweezer array clocks, in which roughly 10-100 individual dipole tweezer traps are loaded into an array with either zero or one atom on each site [7, 25, 26]. The array can then be reconfigured to deterministically realize one atom per site ($P_{\text{filling}} = 1$) [26], or the use of variational quantum algorithms has been proposed to adjust the dynamics on the fly to optimize the generation of spin-squeezing for a given random configuration [27].

In this work we investigate the impact of fractional filling on the degree of spin-squeezing that can be achieved using Rydberg-dressing in the various geometric configurations of optical lattice clocks. We find that fractional filling reduces the achievable degree of squeezing, primarily by increasing the average inter-atomic spacing, with disorder playing only a small role. We consider the impact of random fractionally-filled configurations on the optimal squeezing time and angle of minimal uncertainty, and find that useful levels of squeezing can still be achieved in fractionally filled one-dimensional optical lattices. Finally, we compare the limits on achievable spin-squeezed clock stabilities for the different clock geometries as a function of the number of atoms.

II. SPIN SQUEEZING VIA RYDBERG DRESSING

We analyze the method for generating spin squeezing on the strontium optical clock transition using Rydberg dressing [20] as illustrated in Fig. 1. Figure 1(a) shows the relevant energy level diagram for strontium. In order to simplify our analysis in this work we consider only the stable isotopes of strontium with zero nuclear spin (^{88}Sr, ^{86}Sr,^{84}Sr). In an applied static magnetic field, the doubly-forbidden clock transition between $|g\rangle$ and $|e\rangle$ can be driven with the clock laser and used for Rabi rotations

* kolkowitz@wisc.edu

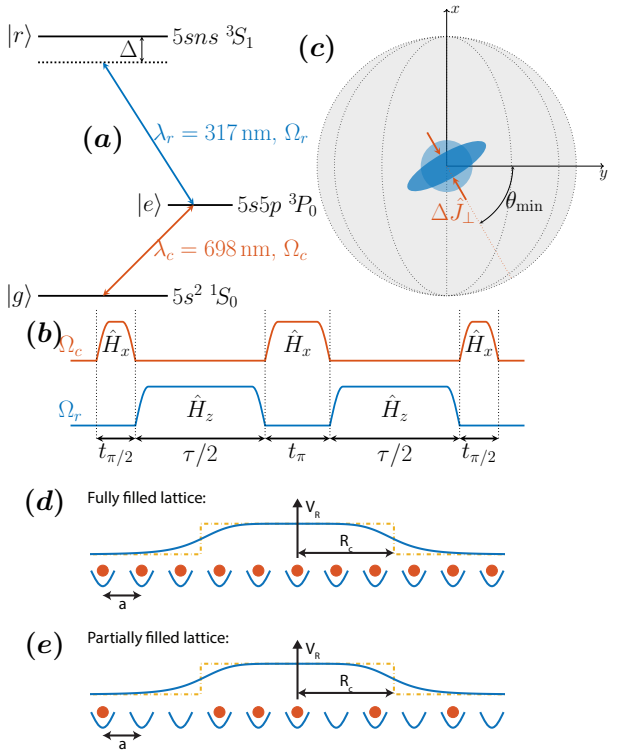

FIG. 1. (a) Strontium energy level diagram. The clock laser drives the transition between $|g\rangle$ and $|e\rangle$ with Rabi frequency Ω_c. The squeezing laser drives the Rydberg transition between $|e\rangle$ and $|r\rangle$ far off-resonance with Rabi frequency Ω_r. (b) Spin-echo sequence of rotation (with the clock transition) and squeezing intervals (with the Rydberg transition) to perform one-axis squeezing of the coherent spin state $|g\rangle^{\otimes N} = |-1/2\rangle^{\otimes N}$. (c) Bottom view of the Bloch sphere illustrating the squeezing of the binomial distribution uncertainty of the coherent spin state towards reduced uncertainty $\Delta\hat{J}_\perp$ along the perpendicular direction at angle $\theta_{\min}$.(d),(e) Fully or partially filled one-dimensional lattice with the dressed Rydberg interaction potential given by Eq. (1) for the central atom (solid line) and the corresponding Heaviside approximation (dashed line).

of the effective two-level atoms. In this effective spin-1/2 picture we define $|g\rangle = |-1/2\rangle$ and $|e\rangle = |+1/2\rangle$ with spin operators $\hat{J}_\alpha = \sum_i \hat{\sigma}_\alpha^{(i)}$, where $\hat{\sigma}_\alpha^{(i)}$ is the Pauli operators $\alpha \in \{x, y, z\}$ acting on atom i. The Rydberg transition between $|e\rangle$ and $|r\rangle$ is driven far off-resonance with one additional Rydberg laser Ω_r. In this regime the frequency detuning Δ of the Rydberg laser from the resonant transition is large, $|\Delta| \gg \Omega_r$, and the Rydberg states are only virtually excited and perturbation theory up to fourth order introduces an energy shift on the $|e\rangle$ energy level that includes an approximate interaction potential between pairs of atoms in the lattice V_{ij} [20, 21, 28–32]:

$$V_{ij} = V(\boldsymbol{r_i}, \boldsymbol{r_j}) = \frac{\hbar\Omega_r^4}{8|\Delta|^3} \frac{R_c^6}{|\boldsymbol{r_i} - \boldsymbol{r_j}|^6 + R_c^6}. \tag{1}$$

This approximate potential has a finite range Rydberg interaction radius $R_c = |C_6/(2\hbar|\Delta|)|^{1/6}$ that spans several lattice sites, illustrated by the solid line above the one-dimensional lattice of Fig. 1(d). The system is described by two Hamiltonians that can be controlled separately, $\hat{H}_x$ from the clock laser and $\hat{H}_z$ from the Rydberg laser:

$$\hat{H}_x = \frac{\hbar\Omega_c}{2} \sum_{i=1}^{N} \hat{\sigma}_x^{(i)}, \tag{2a}$$

$$\hat{H}_z = \sum_{i<j}^{N} \frac{V_{ij}}{4} \hat{\sigma}_z^{(i)} \hat{\sigma}_z^{(j)} + \sum_{i=1}^{N} \frac{\delta_i}{2} \hat{\sigma}_z^{(i)}, \tag{2b}$$

with δ_i the inhomogeneous longitudinal field contributions. Using a spin-echo sequence with the clock laser and Rydberg laser according to Fig. 1(b) on the initial coherent spin state $|g\rangle^{\otimes N} = |-1/2\rangle^{\otimes N}$ removes this unwanted linear procession due to the $\hat{\sigma}_z$ terms, and results in squeezing via one-axis twisting from the effective atom-atom interaction [17, 20]. After the spin-echo sequence, the atom ensemble forms a spin squeezed state with main spin direction along the z-axis and a squeezed uncertainty ellipse with minimal variance along the direction at angle $\theta_{\min}$ illustrated in Fig. 1(c). These spin squeezed states can then be used in a subsequent standard Ramsey clock interrogation sequence (not shown in Fig. 1) along the direction of minimal uncertainty to beat the QPN limit.

The squeezing parameter ξ^2 equals the ratio of the squeezed state variance to the coherent state variance, $\xi^2_{\min}$ is the minimal squeezing parameter along the $\theta_{\min}$ direction obtained with the optimal squeezing time τ_{opt}.

$$\xi^2_{\min} = \frac{N\langle \hat{J}_\perp^2(\theta_{\min})\rangle}{\langle \hat{\boldsymbol{J}}\rangle^2}, \quad \hat{J}_\perp(\theta) = \cos(\theta)\hat{J}_x + \sin(\theta)\hat{J}_y \tag{3}$$

In [20], analytical solutions were derived for the parameters required to evaluate Eq. (3) for the spin-squeezing sequence shown in Fig. 1(b). We present them here:

$$\langle \hat{J}_z \rangle = -\frac{1}{2} \sum_{i=1}^{N} \prod_{k\neq i}^{N} \cos\left(\frac{V_{ij}\tau}{2\hbar}\right) \tag{4a}$$

$$\langle \hat{J}_x^2 \rangle = \frac{N}{4} + \frac{1}{4} \sum_{i<j}^{N} \left[\prod_{k\neq i,j}^{N} \cos\left(\frac{(V_{ik} - V_{jk})\tau}{2\hbar}\right) - \prod_{k\neq i,j}^{N} \cos\left(\frac{(V_{ik} + V_{jk})\tau}{2\hbar}\right) \right] \tag{4b}$$

$$\langle \hat{J}_y^2 \rangle = \frac{N}{4} \tag{4c}$$

$$\langle \hat{J}_x\hat{J}_y + \hat{J}_y\hat{J}_x \rangle = -\sum_{i<j}^{N} \sin\left(\frac{V_{ij}\tau}{2\hbar}\right) \prod_{k\neq i,j}^{N} \cos\left(\frac{V_{ik}\tau}{2\hbar}\right) \tag{4d}$$

While the computation of these terms scales polynomially in the number of atoms in the lattice, it can still be

computationally intensive for large lattices $\geq 10^3$. We have therefore derived exact analytical expressions for these terms in the approximation where the Rydberg interaction potential is replaced with a Heaviside function as illustrated by the dashed curve above the lattice in Fig. 1(d), that can be trivially computed for all lattice sizes $N \geq 2R_c/a$, see appendix B 3. We note that this approximation was previously used in Ref. [29] (without an analytical expression), and as in that work we find that it is a good approximation.

The widely used interaction potential in Eq. (1) is in fact also an approximation based on the assumption that the dipole-dipole interaction between two Rydberg states is dominated by the long range van der Waals contribution $V_{\mathrm{vdW}} \propto 1/r^6$. However in [33] the Rydberg dressing interaction is derived from the dipole-dipole potential V_{dd} including intermediate range $1/r^3$ scaling,

$$V_{\mathrm{dd}} = \frac{\delta}{2} - \frac{\delta}{2}\sqrt{1 + \left(\frac{x_c}{r}\right)^6}, \tag{5a}$$

$$V_{\mathrm{vdW}} = \frac{-\delta}{4}\left(\frac{x_c}{r}\right)^6 = \frac{C_6}{r^6}, \tag{5b}$$

where δ is the Förster defect, and x_c the length scale for the transition from $1/r^3$ to $1/r^6$ scaling of the potential [34]. The corresponding dressed energy shift on the excited clock state $|e\rangle$ will include the exact $V_{ij}(r)$ Rydberg interaction potential presented in Eq. (B1). The quality of the long range van der Waals approximation is strongly dependent on the Förster resonance δ (illustrated by Fig. 6 and Fig. 7 in the appendix).

The Förster energy defects of the ${}^3S_1$ Sr series can be estimated using quantum defect data from Refs. [35, 36]. We have assumed that coupling between triplet and singlet states is negligible and neglected any singlet component of the triplet series.

The defect assuming coupling to ${}^3P_J$ states was calculated from

$$\hbar\delta_J(n) = U(n,{}^3P_J) + U(n-1,{}^3P_J) - 2U(n,{}^3S_1), \tag{6}$$

where the U are term energies $U(n,{}^{(2S+1)}L_J) = -E_H/2[n-\nu_J(n)]^2$ and $\nu_J(n)$ are the n and J dependent quantum defects. For E_H we use the finite mass corrected value of the Hartree energy.

As can be seen in Fig. 8 of appendix B 1, all J channels give a defect that is comparable in magnitude so it is sensible to characterize the interaction with a spin weighted effective value. The spin weighted value was calculated as

$$\delta(n) = \frac{\sum_{J=0,1,2}(2J+1)\delta_J(n)}{\sum_{J=0,1,2} 2J+1}. \tag{7}$$

The $\delta = -1.26\,\mathrm{GHz}$ we calculate for the $5s55s\ {}^3S_1$ Rydberg level results in a potential that is well approximated by V_{ij} of Eq. (1) and we use it for the rest of this work.

It should be noted that this discussion is directly applicable to the bosonic isotopes of Sr which have zero nuclear spin. Rydberg interactions between atoms with hyperfine structure may excite resonances when the hyperfine splitting of the ionic core matches the energy separation of Rydberg levels [37]. Calculations that include the hyperfine structure [38] in ^{87}Sr predict strong resonances leading to orders of magnitude increases in the C_6 coefficent at $n = 64$ and 105. Performing dressing near these values of n may offer a route to enhanced values of R_c/a.

Prior works have argued that far off-resonance Rydberg dressing is advisable due to the improved lifetimes $\tilde{\tau} \propto \Delta^2$ [20, 29]. However, the ratio of the life time to squeezing time $\tilde{\tau}/\tau_{\mathrm{opt}}$ (as well as the degree of squeezing) improves at lower detuning (as shown in appendix A). This means that the far off-resonance regime is not necessarily justified in terms of spin squeezing performance. This conclusion also follows from [33], where a figure of merit for optimal detuning in terms of the ratio between the coherent operation time and state lifetime is defined for one-dimensional lattices. Nevertheless, as with prior works we stay within the far off-resonance regime with $\Delta = -10\Omega_r$ for this work because the resulting spin-squeezing can be treated analytically, and we leave an analysis of the closer-to-resonance case for future work.

III. ONE-DIMENSIONAL LATTICE SQUEEZING

A. Partial Lattice Filling

Prior to this work the achievable spin squeezing via Rydberg dressing has only been studied for fully filled lattices [20, 29], however this condition is not realistic for most optical lattice clocks. In standard one-dimensional optical lattice clocks, atoms are first trapped and cooled with a MOT and then loaded into the lattice potential. After this procedure multiple atoms are present at every lattice site. To protect the clock state from collisional decoherence, a photo-association step can be employed to kick out atoms in pairs from the lattice until only empty or singly occupied sites remain as illustrated by Fig. 1(e). The expected filling probability of each lattice site is $P_{\mathrm{filling}} = 50\%$, and this fractional filling influences the spin squeezing. Similarly, in recent demonstrations of Fermi-degenerate 3D optical lattice clocks the fraction of sites with only one atom is less than unity due to the finite temperature of the atoms when loaded into the lattice [3, 24].

In order to quantify the impact of random fractional filling, we performed simulations on random partially filled one-dimensional lattices with various lattice site filling probabilities $P_{\mathrm{filling}} \in \{0.1, 0.2, ..., 1\}$ using Eq. (4) on a cluster computer. For every simulation, a lattice is randomly filled with the occupation probability of each site equal to P_{filling} and the interactions V_{ij} involving empty sites are made zero in solution Eq. (4). In the simula-

tions shown in Fig. 2 the squeezing time τ and the angle of uncertainty θ are optimized for each individual random lattice configuration. This isolates the impacts of the disorder itself on the achievable spin-squeezing, without the additional constraints of using fixed values for τ and θ. In experiments with optical lattice clocks, shot-to-shot optimizations for each randomly loaded lattice configuration are not practical. We address the impact of instead using more experimentally realistic averaged values for τ_{opt} and θ_{min} in section III C where we find that the system is robust against the small variations in the optimal squeezing time and the angle of minimal uncertainty due to the random variations in each configuration, and show that the effects of these variations can be safely neglected. In Fig. 2(a) the average squeezing parameter $\langle\xi^2_{\text{min}}\rangle$ is plotted for each of the considered filling probabilities using the experimental parameters listed in Table I, with corresponding Rydberg interaction radius of nine lattice sites $R_c/a = 9$ calculated via [35]. The particular parameters used here were selected to be experimentally realistic and representative.

As can be expected, the average minimal squeezing parameter $\langle\xi^2_{\text{min}}\rangle$ scales inversely with the filling probability P_{filling}. Most of the observed variance in squeezing is due to the randomness in the number of atoms loaded into the lattice at a certain filling probability, as can be seen in Fig. 2(b) where we plot the achieved squeezing as a function of the number of atoms randomly loaded into the lattice for each particular simulated configuration that contributed to the averaged values shown in Fig. 2(a).

The dashed lines in Fig. 2(b) represent limiting cases that add perspective to the random fractional filling simulation results. The gold dashed line is the limit where all atoms in the lattice interact with all others with equal interaction strength $V_0 = \frac{\hbar\Omega^4}{8\Delta^3}$ and represents the theoretical best possible squeezing with this one-axis twisting approach. For the minimal squeezing ξ^2_{min} (Eq. (3)), the analytical solution reduces to:

TABLE I.

$\Omega_r/2\pi$	M[a]	a[b]	$\Delta/2\pi$	P_{laser}	ω_0[c]	n[d]
1.6 MHz	10^3	813/2 nm	−16 MHz	300 mW	1 mm	55

[a] M: number of lattice sites, with $N \leq M$ the number of atoms in the lattice
[b] a: Lattice constant fixed by "magic wavelength" $\lambda = 813$ nm
[c] ω_0: Rydberg laser beam waist
[d] n: Rydberg state principal quantum number

$$\langle\hat{J}_z\rangle = \frac{-N}{2}\cos^{N-1}\left(\frac{V_0\tau}{2\hbar}\right), \tag{8a}$$

$$\langle\hat{J}_x^2\rangle = \frac{N}{4} + \frac{N(N-1)}{8}\left(1-\cos^{N-2}\left(2\frac{V_0\tau}{2\hbar}\right)\right), \tag{8b}$$

$$\langle\hat{J}_y^2\rangle = \frac{N}{4}, \tag{8c}$$

$$\langle\hat{J}_x\hat{J}_y + \hat{J}_y\hat{J}_x\rangle = \frac{-N(N-1)}{2}\sin\left(\frac{V_0\tau}{2\hbar}\right)\cos^{N-2}\left(\frac{V_0\tau}{2\hbar}\right). \tag{8d}$$

In this limit the interaction potential has an infinite radius and the squeezing is not influenced by the geometry of the lattice nor by random filling.

In the experimentally relevant case where we are limited by finite-range Rydberg interactions, the optimal possible random fractionally-filled configuration to maximize the degree of squeezing is to place all the atoms next to each other without gaps, as is possible in a tweezer array where the traps can be rearranged to eliminate empty sites. This lower bound corresponds to the purple dashed line in Fig. 2(b).

The inverse scaling of the minimal squeezing parameter ξ^2_{min} with filling fraction can mostly be explained by the increase in average distance between nearest neighbor atoms. The average spacing between atoms in a random fractionally filled lattice is $\langle g\rangle = \frac{a}{P_{\text{filling}}} = \frac{Ma}{\langle N\rangle}$ (with $\langle N\rangle$ the average number of atoms loaded into the lattice at filling probability P_{filling}). It is interesting to compare the random fractionally filled lattice with a fully filled lattice with rescaled lattice constant $a' = \langle g\rangle$. As illustrated by the solid green line in Fig. 2(b), most of the effect of random fractional filling on the spin squeezing can be explained by the average gap in between atoms reducing the effective interaction range R_c/a.

The rescaled lattice model with full filling makes it possible to employ our analytical solution in the Heaviside interaction approximation, which is valid for fully filled lattices. This enables quick estimates of squeezing in random fractionally filled lattices without the need for computationally intensive numerical simulations. The step-like behavior stems from the instant interaction cutoff beyond the Rydberg interaction radius R_c in this approximation. In large fully filled one-dimensional lattice, adding more atoms barely improves the squeezing as illustrated by the lower bound limit in Fig. 2(b). As a result, the Heaviside approximation remains approximately constant until the rescaled lattice gap reduces enough to add an extra atom inside the interaction radius.

The rescaled lattice does not take into account randomly occurring large gaps between separated clusters of atoms. While we do not expect the relative atom positions within a single blockade radius to matter, the total chain contains many clusters of atoms that can easily be disconnected from each other by large gaps at low fractional fillings of the lattice. This explains the remaining

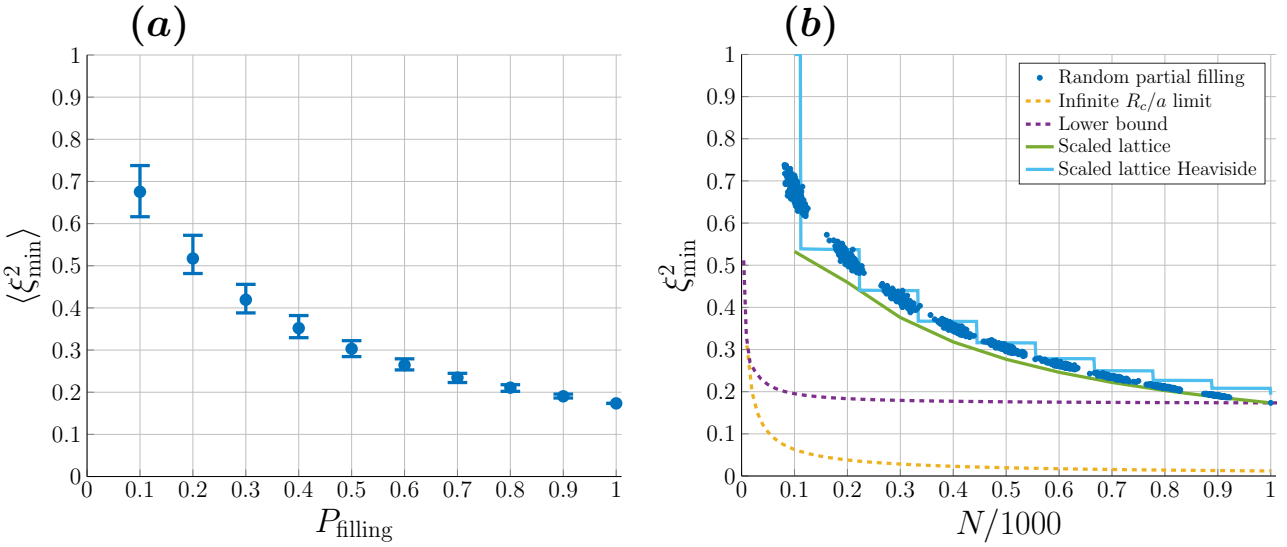

FIG. 2. (a) The minimal squeezing parameter $\xi^2_{\rm min}$ averaged over 200 randomly filled one-dimensional lattice configurations ($M = 10^3$) at each lattice site filling probability $P_{\rm filling} \in \{0.1, 0.2, ..., 1\}$ with Rydberg interaction radius $R_c/a = 9$. The error bars indicate the minimal and maximal value from the simulations. (b) Corresponding scatter plot of minimal squeezing $\xi^2_{\rm min}$ plotted versus the actual filling fraction $N/1000$ loaded into the lattice. The additional solid lines correspond to fully filled lattices with their lattice constant scaled to the average gap size of a randomly filled lattice using the exact interaction potential (green), and with the approximated Heaviside interaction potential (light blue). The dashed lines represent special case limits for fractionally filled lattices: the case where the interaction radius is infinite (gold) and the case when there are no empty sites between the atoms (purple).

variance in the squeezing at fixed filling fraction that can be seen in vertical cross sections of Fig. 2(b), also consistent with larger variances at lower filling fractions where these large gaps become more likely. The actual potential does have non-zero strength at distances beyond R_c and could bridge these gaps and propagate the entanglement throughout separated groups of atoms. However the corresponding interaction strength is so weak that by the time the entanglement has propagated between disconnected chains, the individual clusters of atoms are already 'over squeezed', because $\langle \boldsymbol{J} \rangle$ in Eq. (3) decreases with a prolonged interaction. It is therefore quite fortunate that there is a plateau in $\tau_{\rm opt}$ as a function of the number of atoms, as illustrated by Fig. 7, making it possible for large disconnected clusters with differing atom numbers to simultaneously squeeze to the optimal value within the same interaction time.

The rescaled lattice model captures most of the increase of the squeezing parameter in partially filled lattices, and it also allows for fast estimates through the Heaviside approximation. However because it does not account for large randomly occurring gaps, it still systematically underestimate the increase, as shown by the green line in Fig. 2(b). In appendix C we present better estimates in the form of empirical fitting functions for the average squeezing $\langle \xi^2_{\rm min} \rangle$ Eq. (C1) and squeezing time τ Eq. (C3) in randomly filled one-dimensional lattices with various sizes $M \geq 400$ and interaction radii $R_c/a \in [1; 30]$ as a function of the filling fraction $x = N/M$.

B. Squeezing Time and Rydberg State Decay

In the far off-resonance Rydberg dressing regime, we ignored decay from the finite lifetime Rydberg state $|r\rangle$. A figure of merit for this assumption is the ratio $\tilde{\tau}/\tau_{\rm opt}$, where $\tilde{\tau} = \frac{4\Delta^2}{\Omega_r^2}\tau_{|r\rangle}$ is the enhanced Rydberg state lifetime and $\tau_{|r\rangle} \gtrsim 23\,\mu$s is the lifetime for the strontium Rydberg state with principal quantum number $n = 55$. The simulated optimal squeezing time is $\tau_{\rm opt} \approx 340\,\mu$s for the partially filled one-dimensional lattice experiment considered, resulting in the figure of merit $\frac{\tilde{\tau}}{\tau_{\rm opt}} \approx 27.1 \gg 1$. In [32] the effects of incoherent decay from the Rydberg state on the squeezing are discussed in a simplified treatment. With the assumption that the number of atoms lost due to Rydberg decay equals $\frac{N}{\tilde{\tau}/\tau_{\rm opt}}$, we adopt their approximate estimate for the increase in squeezing parameter as

$$\bar{\xi^2} = \xi^2 + \frac{1}{\tilde{\tau}/\tau_{\rm opt}}. \tag{9}$$

When we apply this estimate to the simulation result of Fig. 2(a) at $P_{\rm filling} = 0.5$, we get $\langle \bar{\xi^2} \rangle \approx 0.337$ which is an increase of 12%. The impact of incoherent Rydberg decay during spin squeezing can be reduced by employing states with higher principal quantum numbers n which have longer life times, or by driving the Rydberg transition closer to resonance to improve the figure of merit $\frac{\tilde{\tau}}{\tau_{\rm opt}}$ as illustrated by Fig. 5 in the appendix. We note

that this simplistic treatment neglects the impact of accidental so-called "spaghetti" resonances between pairs of nearby atoms [39] which may increase the number of Rydberg atoms that are actually generated during dressing, as well as the dephasing that contaminant Rydberg states can induce [40, 41]. We leave these important considerations for future investigation.

C. Randomness and Experimental Parameters

Unlike in tweezer clocks, most optical lattice clocks currently lack single site single-shot atom detection and atom readout is destructive, meaning that the experimental parameters τ and θ_{min} can not be optimized each time the lattice is loaded with another random configuration during clock operation. A fixed average value for τ and θ_{min} must therefore be used, which could potentially reduce the useful degree of squeezing. Fortunately, we find that for realistic parameters the impact of using a fixed squeezing time τ and fixed angle of minimal uncertainty θ_{min} for all random lattice configurations can be neglected, as illustrated by Fig. 3(b). The scatter points for optimized simulations overlap well with the cloud resulting from the well chosen fixed τ and θ_{min} simulations.

To determine the fixed τ, we evaluate the general fitting function Eq. (C3) at half filling $x = 0.5$,

$$\frac{V_0}{\hbar}\tau_{\mathrm{opt,\,fit}}\left(\frac{R_c}{a}\right) = 20.7\left(\frac{R_c}{a}\right)^{-1.49}\left(0.986\cdot(1.016)^{R_c/a}-1\right) + 1.29\left(\frac{R_c}{a}\right)^{-0.635}. \tag{10}$$

We also present the fixed θ_{min} fitting function

$$\theta_{\mathrm{min,fit}}\left(\frac{R_c}{a}\right) = 0.49\exp\left(-0.13\frac{R_c}{a}\right) - 0.49 - \frac{\pi}{4}. \tag{11}$$

This fitting function is illustrated as the dotted line in Fig. 3(a) going through the average optimal angle of minimal uncertainty for random lattice configurations. This approximation is accurate for a wide range of interaction radii $R_c/a \lesssim 30$ for long one-dimensional lattices.

IV. LATTICE CLOCK STABILITY COMPARISON

As discussed above, the achievable degree of squeezing in partially filled lattices is lower than what can be achieved in their fully filled counterparts, which can potentially be constructed with optical tweezers [25, 26]. However, the total number of tweezer traps that can be arranged into a single lattice is currently limited by available laser power to about $N \approx 10^3$ atoms (current experimental demonstrations only reach hundreds of atoms at

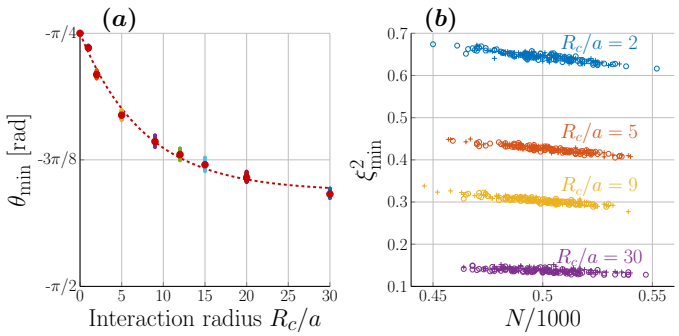

FIG. 3. (a) The angle of minimal uncertainty θ_{min} as illustrated in Fig. 1 plotted for one-dimensional lattices of $M = 1000$ sites, randomly filled with $P_{\mathrm{filling}} = 50\%$. The red line fits to the the average $\langle\theta_{\mathrm{min}}\rangle$ of the random lattice configurations as a function of the Rydberg interaction radius R_c/a. (b) The squeezing ξ^2 obtained in these lattices, where the filled circle data points are the results of simulations with τ_{opt} and θ_{min} optimized for each individual random lattice configuration, while the cross data point simulations used a fixed τ and θ derived from the fitting functions for all the random lattice configurations.

maximum [42]). The number of atoms in optical lattice clocks are limited by a number of factors, including the aforementioned density-dependent collisional shifts, as well inhomogenous broadening due to spatially varying electric and magnetic fields that limit the spatial extent over which atoms in the lattice will remain coherent with each other. Practically speaking this likely limits the atom numbers in one-dimensional lattices to $N \approx 10^3 - 10^4$, while two and three-dimensional lattices can achieve atom numbers in excess of $N \approx 10^6$ [3, 4, 24].

Ultimately, the relevant figure of merit for atomic clocks is not the degree of spin-squeezing, but rather the achievable fractional frequency stability. It may be possible to achieve higher degrees of squeezing with smaller atom numbers, but this does not necessarily correspond to a better clock. To determine the path to a next generation of quantum-enhanced optical atomic clocks, one needs to compare the achievable stability for a given geometry, accounting for limitations on both the achievable spin-squeezing and atom number. Assuming zero-dead time, the clock fractional frequency stability σ can be defined as a function of the averaging time τ_{avg},

$$\sigma(\tau_{\mathrm{avg}}) = \frac{\xi_{\mathrm{min}}}{2\pi\nu_c\sqrt{N}\sqrt{\tau_{\mathrm{avg}}T}}. \tag{12}$$

In Fig. 4 σ is plotted in units of $1/\sqrt{\mathrm{Hz}}$ for fully and fractionally filled strontium optical clocks with clock transition frequency $\nu_c = c/\lambda_c \approx 429.228\,\mathrm{THz}$ and interrogation time $T = 1\,\mathrm{s}$. For the purpose of a fair comparison we assume that the tweezer approach is also able to reach a Rydberg interaction radius of nine lattice sites $R_c/a = 9$, although this requires stronger Rydberg interactions due to the strictly lower lattice con-

stant achievable with tweezers at the clock magic wavelength. As reported in [20], higher dimensional lattices achieve stronger squeezing, and result in better frequency stability. Partially filled one-dimensional lattices with $P_{\text{filling}} = 0.5$ outperform the one-dimensional tweezers for atom numbers $N \geq 2 \cdot 10^3$ (corresponding lattice size $M \geq 4 \cdot 10^3$). The two- and three-dimensional tweezer arrays experience a temporary plateau in the spin squeezing when the lattice size is comparable to the number of atoms inside the Rydberg interaction radius R_c [20]. In this plateau region, the simulations show that the two-dimensional partially filled lattice performance becomes comparable to the three-dimensional lattice. We anticipate that the three-dimensional lattice would start to outperform the two-dimensional lattice again for larger atom numbers (that are computationally inconvenient to simulate). Figure 4 illustrates that identifying the most promising quantum-enhanced optical clock geometry is not trivial and is dependent on the system size.

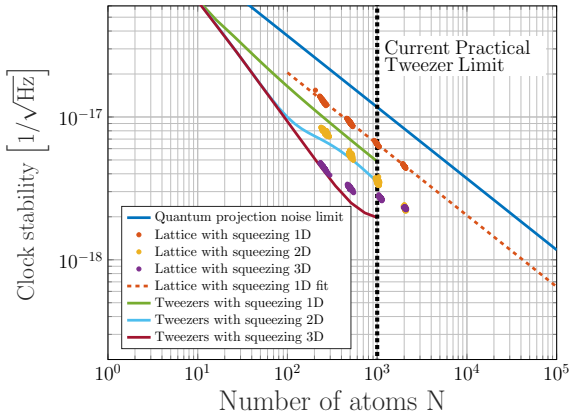

FIG. 4. Simulation results of clock frequency stability as a function of the number of atoms in the lattice. This plot compares the performance of clocks with fully filled tweezer arrays or partially filled lattices ($P_{\text{filling}} = 50\%$) of different dimensionality (1D, 2D, 3D). The dashed fitting function is derived in appendix C and predicts the performance of lattice sizes that are no longer practical to fully simulate. The dotted vertical black line illustrates the rough bound on the number of tweezer traps imposed by current experimentally practical laser powers.

V. CONCLUSION

Spin squeezing via Rydberg dressing is a convenient method with prospects for achieving large degrees of squeezing in state-of-the-art optical lattice clocks. We find that even in the presence of disorder due to random filling, partially filled lattices with larger atom numbers can achieve comparable or superior squeezed clock stabilities compared to the smaller fully filled arrays that can be realized with optical tweezers. The spin squeezing is robust against small deviations in the optimal squeezing time τ and angle of minimal uncertainty θ_{min}, meaning that experiments with fixed τ and θ_{min} for all randomly loaded lattice configurations remain viable. To aid in the practical realization of spin-squeezing via Rydberg-dressing, we have also developed useful approximate methods as tools for experimental implementations in the form of the Heaviside approximation for fully filled one-dimensional lattices, and empirical fitting functions for partially filled one-dimensional lattices.

While we focused only on Rydberg spin-squeezing in a bosonic isotope of Strontium when considering experimental parameters, the analysis presented here is quite general. The principal conclusions regarding the impact of disorder due to imperfect filling on spin-squeezing via finite-range Rydberg interactions are broadly applicable, although care must be taken when making specific approximations of the Rydberg interaction potential. We leave for future exploration the achievable squeezing when the Rydberg laser is brought closer to resonance, and the development of more exotic squeezing sequences to increase the degree of squeezing achievable with finite range interactions.

ACKNOWLEDGMENTS

The authors thank Adam Kaufman and Jeff Thompson for enlightening discussions and helpful comments on the manuscript. This work was supported in part by the NIST Precision Measurement Grants program, the Northwestern University Center for Fundamental Physics and the John Templeton Foundation through a Fundamental Physics grant, the Army Research Office through contract number W911NF1910084, and a Packard Fellowship for Science and Engineering. M.G.V. was supported by DoE BES Materials and Chemical Sciences Research for Quantum Information Science program award No. DE-SC0019449. J. VD acknowledges the support of the Belgian American Educational Foundation (B.A.E.F.) Fellowship.

Appendix A: Optimal Rydberg Detuning

The currently available theory developed to describe spin squeezing with Rydberg dressing requires far off-resonant drive of the Rydberg transition. In this regime the mixture of excited clock states and Rydberg states $|\tilde{e}\rangle \approx |e\rangle - \epsilon\,|r\rangle$ (with $\epsilon = \frac{\Omega_r}{2\Delta}$) has an improved lifetime $\tilde{\tau} = \frac{\tau_{|r\rangle}}{\epsilon^2} \approx \frac{23\,\mu\text{s}}{\epsilon^2}$. Which is argued to be necessary to facilitate long enough squeezing times. To find the optimal detuning of our Rydberg laser, we simulated the obtainable squeezing with the parameters from Table I for a range of detunings Δ.
Note that many influential parameters for spin squeezing depend on the detuning:

$$V_0 = \frac{\hbar\Omega_r^4}{8\Delta^3}$$
$$R_c = \left|\frac{C_6}{2\hbar\Delta}\right|^{1/6} \tag{A1}$$
$$\tilde{\tau} = \frac{4\tau_{|r\rangle}\Delta^2}{\Omega_r^2},$$

with V_0 the interaction potential inside the Rydberg interaction radius R_c and $\tilde{\tau}$ the lifetime of the excited state mixture. Larger V_0 results in shorter optimal squeezing times, while larger interaction radius R_c results in improved squeezing.

The result of the simulations is plotted in Fig. 5. We can conclude that squeezing ξ^2_{min} improves at lower detuning, and surprisingly also the ratio life time to squeezing time $\tilde{\tau}/\tau_{\text{opt}}$ improves at lower detunings. This ratio $\tilde{\tau}/\tau_{\text{opt}}$ is a figure of merit for the assumption that decay from the Rydberg state $|r\rangle$ can be ignored during the squeezing operation.

The far off-resonance regime is not justifiable in terms of spin squeezing performance nor lifetime arguments, and new theory is required to describe the close to resonance regime.

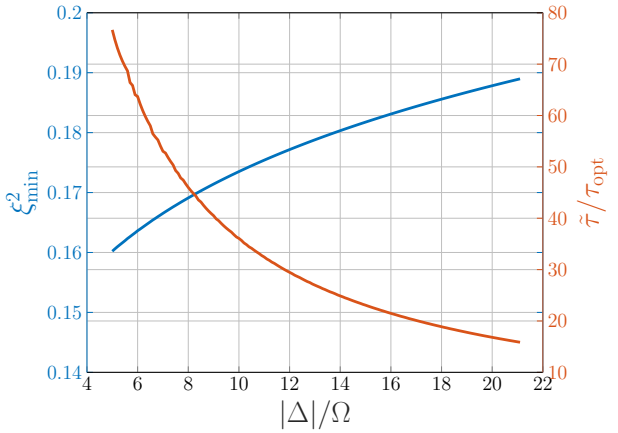

FIG. 5. The squeezing parameter ξ^2_{min} and the figure of merit $\tilde{\tau}/\tau_{\text{opt}}$ as a function of detuning $|\Delta|/\Omega_r$ from the Rydberg transition in a one-dimensional fully filled lattice of $M = 1000$ sites with Rydberg interaction radius $R_c/a = 9$.

Appendix B: Rydberg Interaction Potential

1. Dipole-Dipole Interaction and the van der Waals Approximation

The widely used Rydberg interaction potential of Eq. (1) is in fact an approximation. The interaction between Rydberg atoms is assumed to be dominated by the long range van der Waals approximation $\propto 1/r^6$, while the exact solution derived in [33] also includes the intermediate range dipole-dipole contribution $\propto 1/r^3$. We present this solution below in Eq. (B1):

$$V_{ij}(r) = -\Delta + \frac{V_{dd}}{3} + \frac{2^{2/3}}{f}\left(\Delta^2 - \Delta V_{dd} + V_{dd}^2/3 + |\Omega_r|^2\right) + \frac{2^{1/3} f}{6}. \tag{B1}$$

with

$$V_{dd} = \frac{\delta}{2} - \frac{\delta}{2}\sqrt{1 + \left(\frac{x_c}{r}\right)^6}$$
$$f = \Big[18\Delta V_{dd}(\Delta - V_{dd}) + 4V_{dd}^3 - 9V_{dd}|\Omega_r|^2 + \big[V_{dd}^2(18\Delta^2 - 18\Delta V_{dd} + 4V_{dd}^2 - 9|\Omega_r|^2)^2 - 16(3\Delta^2 - 3\Delta V_{dd} + V_{dd}^2 + 3|\Omega_r|^2)^3\big]^{1/2}\Big]^{1/3}.$$

The Rydberg interaction potential V_{ij} in Eq. (4) arises from the position dependent energy shift of the excited clock state $|e\rangle$ due to the Rydberg dressing including dipole-dipole interactions of the dressed states. At long range, the dipole-dipole interaction is dominated by the van der Waals contribution $\propto 1/r^6$, and approximating the dipole-dipole interaction by just the van der Waals contribution is widely used, however this is not always justified. The simulations presented in Fig. 6 and Fig. 7 show that the Förster defect δ dictates the validity of the van der Waals approximation and δ should be calculated for the specific Rydberg state considered to justify the use of the van der Waals approximation.

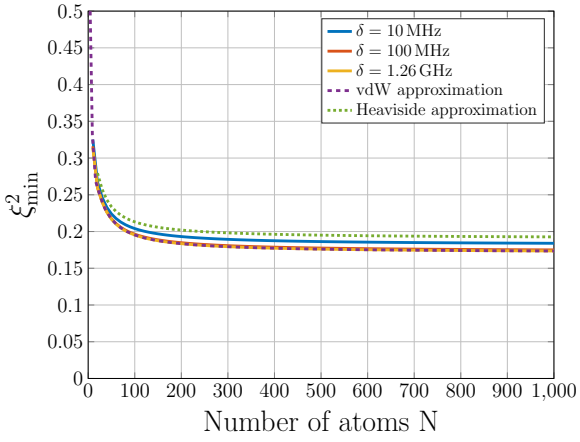

FIG. 6. The squeezing parameter ξ^2_{min} in a one-dimensional fully filled lattice calculated with the solution Eq. (4). We plot the impact of using the exact Rydberg interaction potential V_{ij} of Eq. (B1) with different Förster defects $\delta \in \{10\,\text{MHz}, 100\,\text{MHz}, 1.26\,\text{GHz}\}$ to the van der Waals approximated potential Eq. (1) and the Heaviside solution.

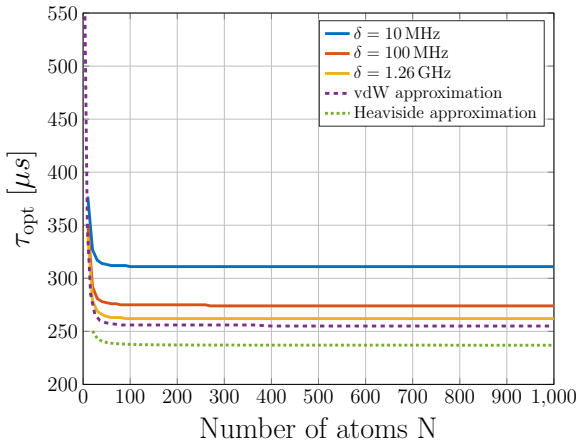

FIG. 7. The optimal squeezing time τ_{opt} in a one-dimensional fully filled lattice calculated with the solution Eq. (4). We plot the impact of using the exact Rydberg interaction potential V_{ij} of Eq. (B1) with different Förster defects $\delta \in \{10\,\mathrm{MHz}, 100\,\mathrm{MHz}, 1.26\,\mathrm{GHz}\}$ to the van der Waals approximated potential Eq. (1) and the Heaviside solution.

The obtainable degree of squeezing is similar throughout the different interaction potentials, however the corresponding optimal squeezing time τ_{opt} is strongly dependent on δ in the exact solution.

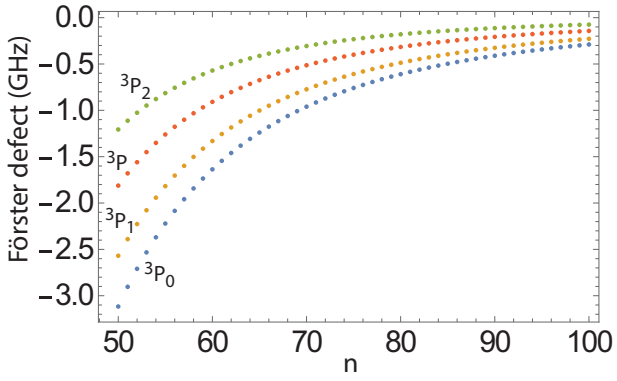

FIG. 8. Förster defect of the $^3S_1$ series in the bosonic isotopes of Sr with nuclear spin zero. Calculations assume coupling to $^3P_{0,1,2}$ (blue, yellow, green dots) and a spin weighted average (red dots).

2. Analytical Solution with Heaviside Approximation

The analytical solution Eq. (4) for spin squeezing via far off-resonance Rydberg dressing in atom lattices scales polynomially in the number of atoms. However for large lattices, this is still computationally very intensive. The interaction potential of the atoms can be approximated by a Heaviside function.

$$V(r) \approx \begin{cases} V_0 = \dfrac{\hbar\Omega_r^4}{8|\Delta|^3} & , \ |r| \leq R_c \\ 0 & , \ \text{otherwise}\,. \end{cases} \tag{B2}$$

With this interaction potential, it is possible to work out all the sums and products of the analytical solution Eq. (4) for one-dimensional lattices and obtain a solution that can be evaluated instantly for all lattice sizes $M \geq 2R_c/a$. Thanks to the binary interaction potential (two atoms either interact with strength V_0 or they don't interact) we can, without loss of generality, assume the interaction radius to be an integer times the lattice constant.
The analytical solution can be simplified using the identity

$$\sum_{k=1}^{K} \cos^k(\phi_0) = \frac{1 - \cos^K(\phi_0)}{1 - \cos(\phi_0)} \tag{B3}$$

By carefully addressing the edges of the lattice and making sure all atom interactions are accounted for, it is possible to evaluate all the summations and products of the analytical solution. The resulting expressions for the observables are presented below.

$$\langle \hat{J}_z \rangle_h = \frac{-1}{2}\left[\left(N - 2\frac{R_c}{a}\right)\cos^{2\frac{R_c}{a}}(\phi_0) + 2\cos^{\frac{R_c}{a}}(\phi_0)\frac{1-\cos^{\frac{R_c}{a}}(\phi_0)}{1-\cos(\phi_0)}\right], \tag{B4a}$$

$$\langle \hat{J}_y^2 \rangle_h = \frac{N}{4}, \tag{B4b}$$

$$\begin{aligned}\langle \hat{J}_x\hat{J}_y + \hat{J}_y\hat{J}_x \rangle_h = &-\left(N - 3\frac{R_c}{a}\right)\frac{R_c}{a}\sin(\phi_0)\cos^{2\frac{R_c}{a}-1}(\phi_0) - \frac{R_c}{a}\sin(\phi_0)\cos^{\frac{R_c}{a}-1}(\phi_0)\frac{1-\cos^{\frac{R_c}{a}}(\phi_0)}{1-\cos(\phi_0)} \\ &-\left(\frac{R_c}{a}\right)^2\sin(\phi_0)\cos^{2\frac{R_c}{a}-1}(\phi_0) - \left(\frac{R_c}{a}-1\right)\sin(\phi_0)\cos^{\frac{R_c}{a}}(\phi_0)\left(\frac{\cos^{\frac{R_c}{a}-1}-1}{\cos(\phi_0)-1}\right) \\ &+\sin(\phi_0)\cos^{\frac{R_c}{a}}(\phi_0)\frac{\frac{R_c}{a}-2+\cos^{\frac{R_c}{a}-1}(\phi_0)-\left(\frac{R_c}{a}-1\right)\cos(\phi_0)}{(\cos(\phi_0)-1)^2},\end{aligned} \tag{B4c}$$

$$\begin{aligned}\langle \hat{J}_x^2 \rangle_h =& \frac{N}{4} + \frac{\left(N-4\frac{R_c}{a}\right)}{4}\frac{\cos^{2\frac{R_c}{a}}(\phi_0)}{\sin^2(\phi_0)}\left[1-\cos^{2\frac{R_c}{a}}(\phi_0)+\cos(2\phi_0)\left(\cos^{\frac{R_c}{a}}(2\phi_0)-\cos^{2\frac{R_c}{a}}(\phi_0)\right)\right] \\ &+\frac{\left(N-3\frac{R_c}{a}\right)}{4}\frac{\cos^2(\phi_0)}{\sin^2(\phi_0)}\left[1-\cos^{2\frac{R_c}{a}}(\phi_0)+\cos^{\frac{R_c}{a}-1}(2\phi_0)\left(\cos^{\frac{R_c}{a}}(2\phi_0)-\cos^{2\frac{R_c}{a}}(\phi_0)\right)\right] \\ &+\frac{1}{2}\Bigg[\left(\frac{R_c}{a}-\frac{\cos^{\frac{R_c}{a}-1}(2\phi_0)}{1-\cos(2\phi_0)}\right)\frac{\cos(\phi_0)\left(1-\cos^{\frac{R_c}{a}}(\phi_0)\right)}{1-\cos(\phi_0)} + \frac{\cos(\phi_0)\cos^{\frac{R_c}{a}-1}(2\phi_0)}{1-\cos(2\phi_0)}\left(\frac{\cos^{\frac{R_c}{a}}(2\phi_0)-\cos^{\frac{R_c}{a}}(\phi_0)}{\cos(2\phi_0)-\cos(\phi_0)}\right) \\ &-\frac{\cos(\phi_0)\left(1-\cos^{\frac{R_c}{a}}(\phi_0)\right)-\frac{R_c}{a}\cos^{\frac{R_c}{a}+1}(\phi_0)(1-\cos(\phi_0))}{(1-\cos(\phi_0))^2} \\ &+\frac{\cos(\phi_0)}{1-\cos(\phi_0)}\Bigg(\frac{\cos^{\frac{R_c}{a}}(\phi_0)-1}{\cos(\phi_0)-1}+\frac{\cos(\phi_0)}{\sin^2(\phi_0)}\left(\cos^{2\frac{R_c}{a}}(\phi_0)-1\right) \\ &-\cos^{\frac{R_c}{a}-1}(2\phi_0)\left(\frac{\cos^{\frac{R_c}{a}}(\phi_0)-\cos^{\frac{R_c}{a}}(2\phi_0)}{\cos(\phi_0)-\cos(2\phi_0)}\right)+\frac{\cos(\phi_0)\cos^{\frac{R_c}{a}-1}(2\phi_0)}{\sin^2(\phi_0)}\left(\cos^{2\frac{R_c}{a}}(\phi_0)-\cos^{\frac{R_c}{a}}(2\phi_0)\right)\Bigg)\Bigg] \\ &+\frac{1}{2}\left[\frac{\cos^{\frac{R_c}{a}}(\phi_0)\left(1-\cos^{\frac{R_c}{a}}(\phi_0)\right)}{\sin^2(\phi_0)(1-\cos(\phi_0))}\left(1-\cos^{2\frac{R_c}{a}}(\phi_0)+\cos(2\phi_0)\left(\cos^{\frac{R_c}{a}}(2\phi_0)-\cos^{2\frac{R_c}{a}}(\phi_0)\right)\right)\right] \\ &+\frac{1+\cos^{2\frac{R_c}{a}-2}(\phi_0)}{4\tan^4(\phi_0)}\left[\frac{\cos^{2\frac{R_c}{a}}(\phi_0)-1}{\cos^2(\phi_0)}+\frac{R_c}{a}\tan^2(\phi_0)\right] \\ &-\frac{\cos^{2\frac{R_c}{a}-2}(\phi_0)\cos(2\phi_0)+\cos^{\frac{R_c}{a}-1}(2\phi_0)}{4\tan^4(\phi_0)}\left[\frac{\cos(2\phi_0)}{\cos^2(\phi_0)}\left(\cos^{2\frac{R_c}{a}}(\phi_0)-\cos^{\frac{R_c}{a}}(2\phi_0)\right)-\frac{R_c}{a}\cos^{\frac{R_c}{a}}(2\phi_0)\tan^2(\phi_0)\right].\end{aligned} \tag{B4d}$$

Figure 9 compares the squeezing parameter calculated with the exact solution to the Heaviside approximation in a fully filled one-dimensional lattice of $M = 10^3$ atoms. To showcase the power of this approximation, we plotted the same Heaviside solution with $M = 10^{12}$ which would be impossible computationally with the exact solution, and is instantly evaluated with the approximation. We conclude that the Heaviside interaction potential is a reasonable approximation with a huge computational advantage. It is worth pointing out that the squeezing becomes almost invariant to the lattice size for large $M \gg 2R_c/a$ one-dimensional lattices.

3. Random Partial Filling with the Heaviside Approximation

We now approximate the Rydberg dressed interaction potential by a Heaviside function in the presence of random partial filling. The difference in optimal squeezing

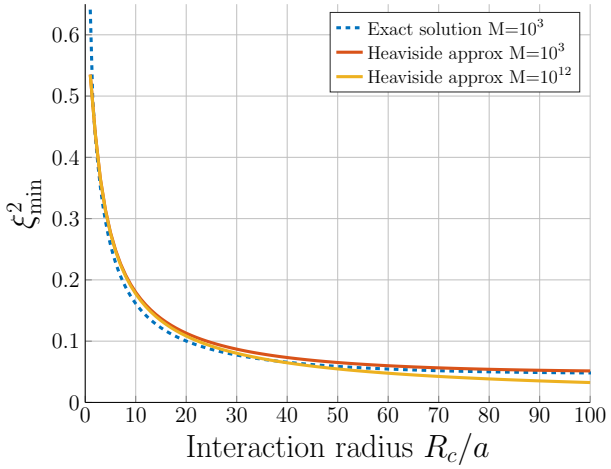

FIG. 9. The squeezing parameter $\xi^2_{\min}$ as a function of the interaction radius R_c/a in a fully filled one-dimensional lattice of size M.

time and squeezing parameter between the Heaviside approximation and actual potential is illustrated in Fig. 10. The effect of the random lattice filling is very similar for the finite range Heaviside potential, agreeing with our intuitive explanation in section III A where we already noted that the entanglement does not propagate beyond gaps larger than R_c. There is however an offset of $\approx 10\%$ on both the optimal squeezing time and the squeezing parameter compared to the exact solution, justifying the use of the actual potential in all our simulations.

Appendix C: Empirical Fitting Functions for Random Partial Filling of One-dimensional Lattices

Squeezing is influenced by the statistics of the random lattice configurations. In the absence of a physical model describing these statistics properly, we can derive empirical fitting functions to describe the squeezing $\xi^2_{\min}$ and the optimal squeezing time τ_{opt} for randomly filled one-dimensional lattices with various sizes and interaction radii R_c/a. These fitting functions are a useful tool to predict squeezing in randomly filled one-dimensional lattices without the need for simulations on cluster computers. We refer to the number of lattice sites as M, the number of atoms inside the lattice as N, with $N \leq M$ and the filling fraction $x = N/M$.

We anticipate the squeezing parameter to be a function of the lattice size, the filling fraction and the interaction radius: $\xi^2_{\min}(R_c/a, M, x)$. The fitting function has the general form of Eq. (C1) where the dependence on R_c/a and M is hidden in the fitting parameters $\{\alpha, \beta, \gamma, \lambda\}$:

$$\xi^2_{\min}(R_c/a, M, x) = \alpha \exp(-\beta x) + \gamma \exp(-\lambda x). \quad \text{(C1)}$$

From the requirement $\lim_{x\to 0} \xi^2_{\min} = 1$ we can eliminate one degree of freedom in Eq. (C1): $\gamma = 1 - \alpha$.

From simulations at full filling $x = 1$ we conclude that the squeezing is approximately independent of M in the case of large lattices ($M \gtrsim 400$), this breaks down for very large $\frac{R_c}{a}$ (comparable to the system size), which we can ignore for the type of experiments we are considering. This means we can remove the dependence on M in our fit and impose the dependence on R_c/a at full filling with

$$\xi^2_{\min}(\frac{R_c}{a}, x = 1) = 0.6571\,(R_c/a)^{-0.656} + 0.01197$$

by fitting to Fig. 9 (note that we could have worked out an expression based on the Heaviside solution, but this would have been too bulky). We express the remaining fitting parameters $\{\beta, \lambda\}$ as functions of R_c/a by fitting to multiple random filling simulations at different interaction radii. The resulting fitting parameter values are listed in Eq. (C2).

$$\alpha = \frac{0.657\left(\frac{R_c}{a}\right)^{-0.656} + 0.01197 - \exp(-\lambda)}{\exp(-\beta) - \exp(-\lambda)}, \quad \text{(C2a)}$$

$$\beta = 0.293\frac{R_c}{a} + 5.297, \quad \text{(C2b)}$$

$$\gamma = 1 - \alpha, \quad \text{(C2c)}$$

$$\lambda = 1.14 - 2\exp\left(-0.89\frac{R_c}{a}\right). \quad \text{(C2d)}$$

Figure 11 illustrates the fitting function of Eq. (C1) for different interaction radii $R_c/a \in \{2, 5, 9, 30\}$. The fits perform well and can be evaluated instantly to predict the average squeezing obtainable in randomly filled one-dimensional lattices of various sizes $M \geq 400$ and with various interaction radii $\frac{R_c}{a} \in [1; 30]$, instead of performing hundreds/thousands of simulations taking several hours each. Similarly we present a fitting function for the corresponding optimal squeezing times Eq. (C3).

$$\frac{V_0}{\hbar}\tau_{\text{opt}}\left(\frac{R_c}{a}, M, x\right) = \mu x^{-\nu} + 1.29\left(\frac{R_c}{a}\right)^{-0.635} - \mu,$$
$$\mu = 20.7\left(\frac{R_c}{a}\right)^{-1.49}, \quad \nu = 0.0229\frac{R_c}{a} - 0.0198. \quad \text{(C3)}$$

The performance of fitting function Eq. (C3) is illustrated in Figure 12, and performs well except for small filling fractions where the variance of optimal squeezing time τ_{opt} for randomly filled lattices becomes large.

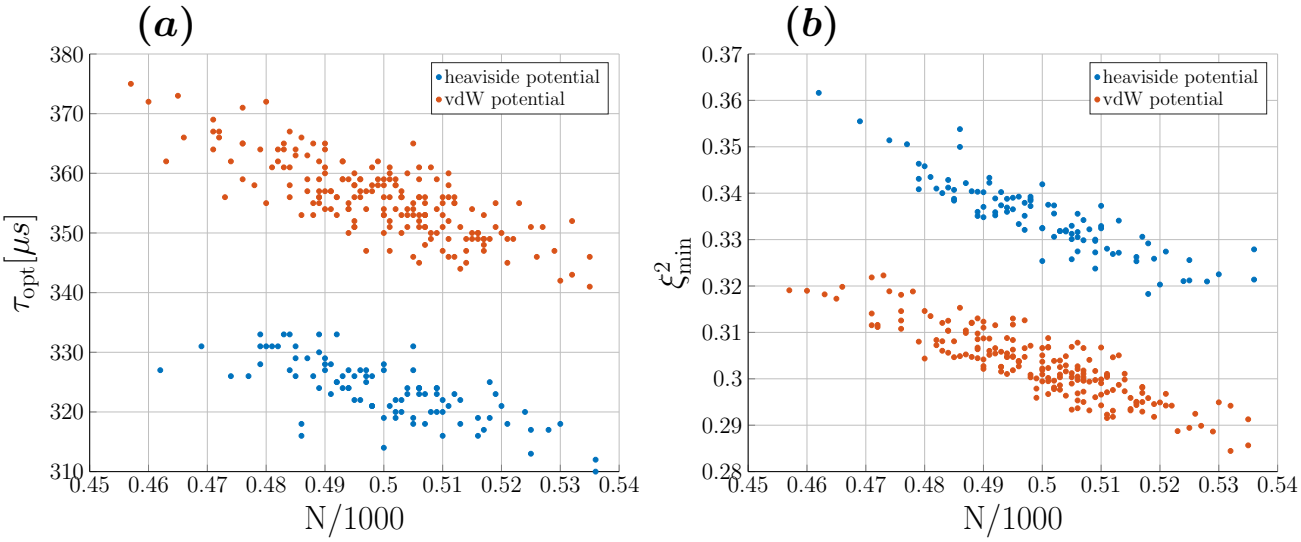

FIG. 10. (a) The optimal squeezing time τ_{opt} for 100 randomly filled one-dimensional lattice configurations ($M = 10^3$) at lattice site filling probability $P_{\mathrm{filling}} = 0.5$ with Rydberg interaction radius $R_c/a = 9$. We compare the actual interaction potential with the Heaviside approximation. (b) Corresponding scatter plot of minimal squeezing ξ^2_{min} plotted versus the actual filling fraction $N/1000$ loaded into the lattice.

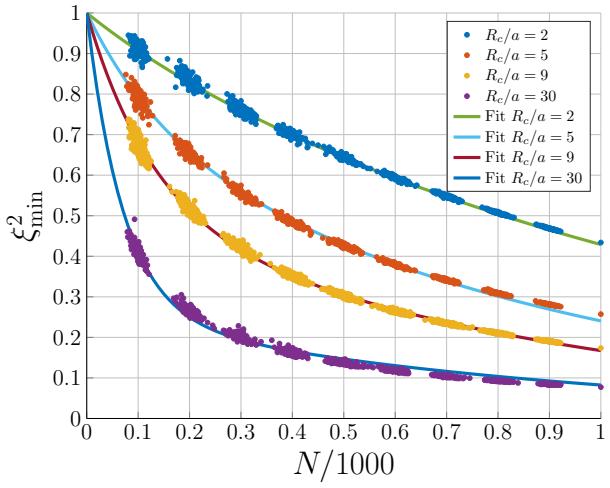

FIG. 11. The squeezing parameter ξ^2_{min} in random fractionally filled one-dimensional lattices of size $M = 10^3$ simulated for different Rydberg interaction radii R_c together with the corresponding fitting function from Eq. (C1).

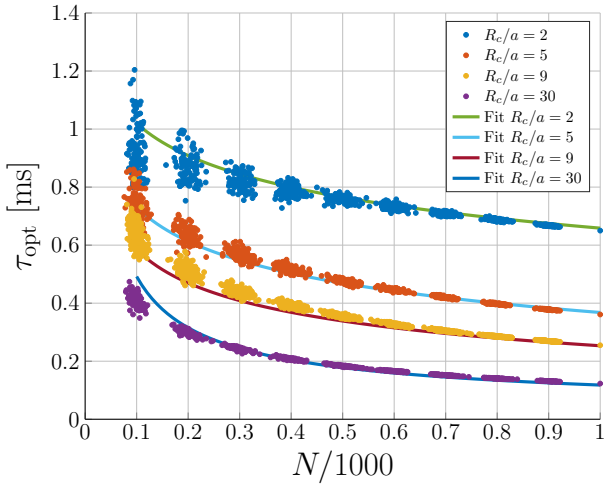

FIG. 12. The optimal squeezing time τ_{opt} in random fractionally filled one-dimensional lattices of size $M = 10^3$ simulated for different Rydberg interaction radii R_c together with the corresponding fitting function from Eq. (C3).

[1] B. Bloom, T. Nicholson, J. Williams, S. Campbell, M. Bishof, X. Zhang, W. Zhang, S. Bromley, and J. Ye, An optical lattice clock with accuracy and stability at the 10^{-18} level, Nature **506**, 71 (2014).

[2] T. Bothwell, D. Kedar, E. Oelker, J. Robinson, S. Bromley, W. Tew, J. Ye, and C. Kennedy, JILA SrI optical lattice clock with uncertainty of 2.0×10^{-18}, Metrologia **56**, 065004 (2019).

[3] G. E. Marti, R. B. Hutson, A. Goban, S. L. Campbell, N. Poli, and J. Ye, Imaging optical frequencies with 100 μHz precision and 1.1 μm resolution, Phys. Rev. Let. **120**, 103201 (2018).

[4] E. Oelker, R. Hutson, C. Kennedy, L. Sonderhouse, T. Bothwell, A. Goban, D. Kedar, C. Sanner, J. Robinson, G. Marti, et al., Demonstration of 4.8×10^{-17} stability at 1 s for two independent optical clocks, Nature Photonics **13**, 714 (2019).

[5] D. B. Hume and D. R. Leibrandt, Probing beyond the laser coherence time in optical clock comparisons, Phys. Rev. A **93**, 032138 (2016).

[6] T. R. Tan, R. Kaewuam, K. J. Arnold, S. R. Chanu, Z. Zhang, M. Safronova, and M. D. Barrett, Suppressing inhomogeneous broadening in a lutetium multi-ion optical clock, Phys. Rev. Let. **123**, 063201 (2019).

[7] A. W. Young, W. J. Eckner, W. R. Milner, D. Kedar, M. A. Norcia, E. Oelker, N. Schine, J. Ye, and A. M. Kaufman, A tweezer clock with half-minute atomic coherence at optical frequencies and high relative stability, arXiv preprint arXiv:2004.06095 (2020).

[8] E. R. Clements, M. E. Kim, K. Cui, A. M. Hankin, S. M. Brewer, J. Valencia, J.-S. Chen, C.-W. Chou, D. R. Leibrandt, and D. B. Hume, Lifetime-limited interrogation of two independent $^{27}Al^{+}$ clocks using correlation spectroscopy, arXiv preprint arXiv:2007.02193 (2020).

[9] M. Takamoto, I. Ushijima, N. Ohmae, T. Yahagi, K. Kokado, H.-a. Shinkai, and H. Katori, Test of general relativity by a pair of transportable optical lattice clocks, Nature Photonics **14**, 411 (2020).

[10] I. Counts, J. Hur, D. P. A. Craik, H. Jeon, C. Leung, J. C. Berengut, A. Geddes, A. Kawasaki, W. Jhe, and V. Vuletić, Evidence for nonlinear isotope shift in Yb^{+} search for new boson, Phys. Rev. Let. **125**, 123002 (2020).

[11] A. Ludlow, M. Boyd, J. Ye, E. Peik, and P. Schmidt, Optical atomic clocks, Reviews of Modern Physics **87**, 637 (2015).

[12] T. Takano, M. Takamoto, I. Ushijima, N. Ohmae, T. Akatsuka, A. Yamaguchi, Y. Kuroishi, H. Munekane, B. Miyahara, and H. Katori, Geopotential measurements with synchronously linked optical lattice clocks, Nature Photonics **10**, 662 (2016).

[13] N. Huntemann, B. Lipphardt, C. Tamm, V. Gerginov, S. Weyers, and E. Peik, Improved limit on a temporal variation of m_p/m_e from comparisons of Yb^{+} and Cs atomic clocks, Phys. Rev. Lett. **113**, 210802 (2014).

[14] S. Kolkowitz, I. Pikovski, N. Langellier, M. D. Lukin, R. L. Walsworth, and J. Ye, Gravitational wave detection with optical lattice atomic clocks, Phys. Rev. D **94**, 124043 (2016).

[15] V. Giovannetti, S. Lloyd, and L. Maccone, Quantum-enhanced measurements: Beating the standard quantum limit, Science (New York, N.Y.) **306**, 1330 (2004).

[16] L. Pezzè, A. Smerzi, M. K. Oberthaler, R. Schmied, and P. Treutlein, Quantum metrology with nonclassical states of atomic ensembles, Rev. Mod. Phys. **90**, 035005 (2018).

[17] M. Kitagawa and M. Ueda, Squeezed spin states, Phys. Rev. A **47**, 5138 (1993).

[18] O. Hosten, N. J. Engelsen, R. Krishnakumar, and M. A. Kasevich, Measurement noise 100 times lower than the quantum-projection limit using entangled atoms, Nature **529**, 505 (2016).

[19] E. Pedrozo-Peafiel, S. Colombo, C. Shu, A. F. Adiyatullin, Z. Li, E. Mendez, B. Braverman, A. Kawasaki, D. Akamatsu, Y. Xiao, and V. Vuleti, Entanglement-enhanced optical atomic clock (2020), arXiv:2006.07501.

[20] L. I. R. Gil, R. Mukherjee, E. M. Bridge, M. P. A. Jones, and T. Pohl, Spin squeezing in a Rydberg lattice clock, Phys. Rev. Lett. **112**, 103601 (2014).

[21] V. Borish, O. Markovi, J. Hines, S. Rajagopal, and M. Schleier-Smith, Transverse-field Ising dynamics in a Rydberg-dressed atomic gas, Phys. Rev. Let. **124** (2020).

[22] I. S. Madjarov, J. P. Covey, A. L. Shaw, J. Choi, A. Kale, A. Cooper, H. Pichler, V. Schkolnik, J. R. Williams, and M. Endres, High-fidelity entanglement and detection of alkaline-earth Rydberg atoms, Nature Physics , 857 (2020).

[23] T. Nicholson, S. Campbell, R. Hutson, G. Marti, B. Bloom, R. McNally, W. Zhang, M. Barrett, M. Safronova, G. Strouse, et al., Systematic evaluation of an atomic clock at $2{\times}10^{-18}$ total uncertainty, Nature communications **6**, 6896 (2015).

[24] S. L. Campbell, R. Hutson, G. Marti, A. Goban, N. D. Oppong, R. McNally, L. Sonderhouse, J. Robinson, W. Zhang, B. Bloom, et al., A Fermi-degenerate three-dimensional optical lattice clock, Science **358**, 90 (2017).

[25] I. S. Madjarov, A. Cooper, A. L. Shaw, J. P. Covey, V. Schkolnik, T. H. Yoon, J. R. Williams, and M. Endres, An atomic-array optical clock with single-atom readout, Phys. Rev. X **9**, 041052 (2019).

[26] M. Endres, H. Bernien, A. Keesling, H. Levine, E. R. Anschuetz, A. Krajenbrink, C. Senko, V. Vuletic, M. Greiner, and M. D. Lukin, Atom-by-atom assembly of defect-free one-dimensional cold atom arrays, Science **354**, 1024 (2016).

[27] R. Kaubruegger, P. Silvi, C. Kokail, R. van Bijnen, A. M. Rey, J. Ye, A. M. Kaufman, and P. Zoller, Variational spin-squeezing algorithms on programmable quantum sensors, Phys. Rev. Let. **123**, 260505 (2019).

[28] J. E. Johnson and S. L. Rolston, Interactions between Rydberg-dressed atoms, Phys. Rev. A **82**, 033412 (2010).

[29] M. Khazali, H. W. Lau, A. Humeniuk, and C. Simon, Large energy superpositions via Rydberg dressing, Phys. Rev. A **94**, 023408 (2016).

[30] J. Zeiher, R. Van Bijnen, P. Schauß, S. Hild, J.-y. Choi, T. Pohl, I. Bloch, and C. Gross, Many-body interferometry of a Rydberg-dressed spin lattice, Nature Physics **12**, 1095 (2016).

[31] N. Henkel, R. Nath, and T. Pohl, Three-dimensional roton excitations and supersolid formation in Rydberg-excited Bose-Einstein condensates, Phys. Rev. Lett. **104**, 195302 (2010).

[32] I. Bouchoule and K. Mlmer, Spin squeezing of atoms by

the dipole interaction in virtually excited Rydberg states, Phys. Rev. A **65** (2002).
[33] M. Saffman, Quantum computing with atomic qubits and Rydberg interactions: progress and challenges, Journal of Physics B: Atomic, Molecular and Optical Physics **49**, 202001 (2016).
[34] T. G. Walker and M. Saffman, Consequences of Zeeman degeneracy for the van der Waals blockade between Rydberg atoms, Phys. Rev. A **77**, 032723 (2008).
[35] C. L. Vaillant, M. P. A. Jones, and R. M. Potvliege, Long-range Rydberg–Rydberg interactions in calcium, strontium and ytterbium, Journal of Physics B: Atomic, Molecular and Optical Physics **45**, 135004 (2012).
[36] R. Ding, J. D. Whalen, S. K. Kanungo, T. C. Killian, F. B. Dunning, S. Yoshida, and J. Burgdörfer, Spectroscopy of ^{87}Sr triplet Rydberg states, Phys. Rev. A **98**, 042505 (2018).
[37] F. Robicheaux, D. W. Booth, and M. Saffman, Theory of long range interactions for Rydberg states attached to hyperfine split cores, Phys. Rev. A **97**, 022508 (2018).
[38] F. Robicheaux, Calculations of long range interactions for ^{87}Sr Rydberg states, J. Phys. B: At. Mol. Opt. Phys. **52**, 244001 (2019).
[39] Y.-Y. Jau, A. Hankin, T. Keating, I. Deutsch, and G. Biedermann, Entangling atomic spins with a Rydberg-dressed spin-flip blockade, Nature Physics **12**, 71 (2016).
[40] E. A. Goldschmidt, T. Boulier, R. C. Brown, S. B. Koller, J. T. Young, A. V. Gorshkov, S. Rolston, and J. V. Porto, Anomalous broadening in driven dissipative Rydberg systems, Phys. Rev. Let. **116**, 113001 (2016).
[41] T. Boulier, E. Magnan, C. Bracamontes, J. Maslek, E. Goldschmidt, J. Young, A. V. Gorshkov, S. Rolston, and J. V. Porto, Spontaneous avalanche dephasing in large Rydberg ensembles, Phys. Rev. A **96**, 053409 (2017).
[42] D. Barredo, V. Lienhard, S. de Léséleuc, T. Lahaye, and A. Browaeys, Synthetic three-dimensional atomic structures assembled atom by atom, Nature **561**, 79 (2018).